Mon. Not. R. Astron. Soc. **000**, 000–000 (0000) Printed 6 May 2013 (MN LATEX style file v2.2)

A non-parametric method for mass modelling spherical systems

P. Steger[1⋆], D. von Rickenbach[1], J. I. Read[1,2]
[1] *Institute for Astronomy, Department of Physics, ETH Zürich, Wolfgang-Pauli-Strasse 27, CH-8093 Zürich, Switzerland*
[2] *Department of Physics, University of Surrey, Guildford, GU2 7XH, UK*

6 May 2013

ABSTRACT

We propose a new non-parametric method to determine the mass distribution in spherical systems. A high dimensional parameter space encoding tracer density, line of sight velocity dispersion and total mass density is sampled with an Monte Carlo Markov Chain.

Without assumptions on the functional form of any of these profiles, we can reproduce liably the total mass density of mock dwarf galaxies, and disentangle the degeneracy between dark matter density and tracer velocity anisotropy.

We show early applications to observed dwarf galaxies, and point out what data quality is required to yield a sensible estimate.

Key words: galaxies: dwarf – galaxies: fundamental parameters – galaxies: kinematics and dynamics – cosmology: dark matter

1 INTRODUCTION

Cosmological ΛCDM simulations of representative patches of the Universe predict the dark matter to assemble self-similarly.

Assuming that only dark matter might influence the physics on all scales down to the stellar regime, Navarro et al. (1997) found that the density profiles of the resulting halos are best described by a function diverging as r^{-1} towards the center. Given that only a finite amount of dark matter is available in the halo, there exists a very small lower bound for a turnover radius, where the density approaches a constant value.

Observations of low surface brightness galaxies measure rotation curves and deduce from them a constant density below a rather large scale radius r_S (de Blok et al. 2001), (McGaugh et al. 2001), contrary to the theoretical predictions.

This fact became known as the cusp/core problem.

Many solutions have been proposed to solve it. It was deemed possible that difficulties in data modelling prevent observations from resolving cusps.

From a theoretical point, it was proposed that dark matter is not cold as assumed, with a warm component smearing out density peaks below a certain scale.

Dark matter could also be self-interacting, as e.g. postulated by (Spergel & Steinhardt (2000), Vogelsberger et al. (2012)), and have a large scattering cross-section and low annihilation or dissipation cross-section, and thus prevent formation of overly-dense cusps.

For the simulations in question, it became clear that baryonic physics plays a crucial role for the buildup of the overall density profile on small scales, and thus dark matter.

In particular, modelling of stellar feedback, the introduction of a higher density threshold for star formation and an increase of resolution for treatment of individual star-forming regions in a cosmological context led simulations to reveal dwarf galaxies with shallow central density slopes in dark matter (Governato et al. 2010). This compares well with what is found in THINGS dwarf galaxies (Oh et al. 2011).

Another type of dwarf galaxies, the dwarf spheroidals, lie closer to the Sun and can be resolved much better, often allowing us to observe individual stars. We need a method to model their mass distribution from those observations to investigate, whether they exhibit a cusp or a core, and whether simulations are able to reproduce the dark matter distribution.

An early approach for general triaxial systems in dynamical equilibrium was proposed by Schwarzschild (1979): Based on a density profile and a corresponding gravitational potential, an ensemble of orbits are calculated and superposed to yield the underlying density profile.

Another method makes use of the Jeans equations encompassing tracer density, velocity dispersion and the gravitational potential to solve for the potential, and ultimately get the underlying dark matter density (Binney & Tremaine 2008). Mostly, a functional form with some free parameter(s)

⋆ E-mail: psteger@phys.ethz.ch

is assumed for the density profile, and fitting routines are used to yield the best agreeing form.

Another assumption is required for the velocity anisotropy profile to get a mass density in the case of lowest-order Jeans equations. Since it is not known a priori how much the system is supported by rotational motion, this leads to a degeneracy between mass and velocity anisotropy.

Higher order Jeans equations can help to break this degeneracy (Łokas 2002). Another degeneracy between inner DM slope and concentration shows up, though. With better data available for the local dSphs, distribution function based methods may be used. Breddels et al. (2012) cannot distinguish between cuspy or cored profiles for Sculptor.

Yet another approach is to use the motion of globular clusters inside dwarf galaxies (Goerdt et al. 2006), (Cole et al. 2012). If the density distribution follows a cored profile, globular clusters will not fall in, or will even get pushed out of the core if they formed inside. In Fornax dSph, there is evidence for a core.

Walker & Peñarrubia (2011) split the stellar tracers into two populations with different metallicities and half-mass radii, and make use of the fact that the enclosed mass is found the same at the half-mass radius, independent of the underlying velocity anisotropy profile, to get two points in the center of the dwarf galaxy, from which constraints on the inner DM density slope can be drawn.

We want to get the full density profile, though.

In this paper, we propose a new non-parametric mass-modelling technique based on the Jeans approach, with no assumptions on the functional form of the dark matter density, nor the velocity anisotropy profile.

We assume spherical symmetry in a first step. Beware that dSph galaxies of the local group are known to be slightly non-spherical, with an average ellipticity of 0.3 (Mateo 1998).

Our method has following advantages over other methods presented so far:

(i) no assumptions on the functional form of the underlying dark matter;
(ii) applicable to any gravitational model, since Jeans equation and Poisson equation are solved each on their own;
(iii) robust to noise in the data, as no numerical differentiation is used as soon as the three-dimensional model stands.

2 METHOD

The collisionless Boltzmann equation for a spherical system with gravitational potential Φ,

$$\frac{\mathrm{d}f}{\mathrm{d}t} = \frac{\partial f}{\partial t} + \nabla_{\vec{x}} f \cdot \vec{v} - \nabla_{\vec{v}} f \cdot \nabla_{\vec{x}} \Phi = 0, \tag{1}$$

describes the motion of tracer stars with distribution function $f(\vec{x}, \vec{v})$.

In spherical coordinates (r, θ, ϕ), the collisionless Boltzmann equation then reads as

$$\frac{\partial f}{\partial t} + \dot{r}\frac{\partial f}{\partial r} + \dot{\theta}\frac{\partial f}{\partial \theta} + \dot{\phi}\frac{\partial f}{\partial \phi} + \dot{v}_r\frac{\partial f}{\partial v_r} + \dot{v}_\theta\frac{\partial f}{\partial v_\theta} + \dot{v}_\phi\frac{\partial f}{\partial v_\phi} = 0 \tag{2}$$

with velocities

$$\dot{r} = v_r, \tag{3}$$
$$\dot{\theta} = v_\theta / r \tag{4}$$
$$\dot{\phi} = v_\phi / r \sin\theta. \tag{5}$$

The assumption of steady state hydrodynamic equilibrium gives $\partial f/\partial t = 0$ and $\bar{v}_r = 0$, and using spherical symmetry $\bar{v}_\theta = 0$, $\bar{v}_\phi = 0$, with a unique tangential velocity dispersion $\sigma_\phi^2 = \sigma_\theta^2 = \sigma_t^2$ yields

$$\frac{1}{\nu}\frac{\partial}{\partial r}(\nu\sigma_r^2) + 2\frac{\sigma_r^2 - \sigma_t^2}{r} = -\frac{\partial \Phi}{\partial r} = -\frac{GM(<r)}{r^2} \tag{6}$$

with enclosed mass $M(<\ r)$, gravitational constant $G = 6.67398 \cdot 10^{-11}\mathrm{m}^3/\mathrm{kg\,s}^2$. The departure from spherical hydrostatic equilibrium $\sigma_r^2 = \sigma_t^2$ is measured by the anisotropy parameter

$$\beta \equiv 1 - \frac{\sigma_t^2}{\sigma_r^2} \tag{7}$$

with values in the range from $-\infty$ (purely circular orbits) through 0 (hydrostatic equilibrium) to 1 (purely radial orbits).

Integrating both sides of equation 6 gives the main equation of this paper,

$$\sigma_r^2(R) = \frac{1}{\nu(R)} \exp\left(-2\int_{r_{min}}^{r} \frac{\beta(s)}{s}\mathrm{d}s\right) \cdot \tag{8}$$

$$\int_R^\infty \frac{GM(r)\nu(r)}{r^2} \exp\left(2\int_{r_{min}}^{r} \frac{\beta(s)}{s}\mathrm{d}s\right)\mathrm{d}r.$$

For distant spherical systems, only the projected velocity dispersion σ_{LOS} can be measured, which in our case is given by

$$\sigma_{\mathrm{LOS}}^2(R) = \frac{2}{\Sigma(R)}\int_R^\infty \left(1 - \beta\frac{R^2}{r^2}\right)\frac{\nu(r)\sigma_r^2(r)r}{\sqrt{r^2 - R^2}}\mathrm{d}r, \tag{9}$$

where $\Sigma(R)$ denotes the surface mass density at radius R.

In the following, we present a fully non-parametric method for the solution of equation 9 for the total gravitating mass density $\rho(r)$, given observed $\nu(r)$ and $\sigma_{\mathrm{LOS}}(r)$, where r denotes the projected two-dimensional radius from the center of mass of the spherical system. We get the enclosed mass $M(<r)$ from the density via

$$M(<r) = \int_0^r \rho(r) r^2 dr, \tag{10}$$

which shows up in eq. 8. In principle, the above-mentioned method can be generalized to investigate alternative gravity models, if the acceleration $GM(r)/r^2$ is replaced with the respective form of $-\partial\Phi/\partial r$.

The degeneracy between mass M and velocity anisotropy β is accounted for: For any non-isothermal system, we let vary the anisotropy $\beta(r)$ as well. We checked that in the case of a simple Hernquist profile, $\beta(r) \approx 0$ is retrieved correctly.

The main idea is to let an Monte Carlo Markov Chain

sample the parameter space $[\nu_i, \sigma_{\rm LOS,i}, \rho]$ for distinct populations $i = 1...N$ of stellar or gaseous tracers.

Two different approaches are taken into account for the sampling of densities:

Tracer densities ν_i are expected to fall with increasing radii. To ensure this, one can explicitly build a monotonic function

$$\nu_i(r) = \int_0^r \tilde{\nu}_i(r')dr' \tag{11}$$

with parameters $\tilde{\nu}_i(r') > 0$ discretized in bins. The other possibility is to let $\tilde{\nu}_i(r')$ vary freely, or just sample $\nu_i(r') = \tilde{\nu}_i|_{r'}$ directly. As it turns out, the MCMC prefers decreasing densities anyhow, so the ν_i parameters were allowed to vary within the priors described below.

Furthermore, the sampling might be done in a linear or logarithmic fashion. Wherever negative components are required, $\beta_i(r)$, linear sampling was chosen, s.t.

$$\beta_i^{(n+1)}(r) = \beta_i^{(n)}(r) + \delta\beta_i(r) \tag{12}$$

with new parameter $\beta_i^{(n+1)}(r)$ in iteration $n+1$ determined from its old value $\beta_i^{(n)}(r)$ at iteration n and the parameter stepsize $\delta\beta_i(r)$ drawn from a random uniform distribution. On the other hand, for any positive definite parameter that needs to span a range in logarithmic space, $\nu_i(r)$ and $\rho(r)$, we sample logarithmically,

$$\nu_i^{(n+1)}(r) = 10^{\tilde{\nu}_i^{(n+1)}}, \qquad \tilde{\nu}_i^{(n+1)}(r) = \tilde{\nu}_i^{(n)}(r) + \delta\tilde{\nu}_i(r) \tag{13}$$

In a next step, $\sigma_{\rm LOS,i}(r)$ is calculated from ν_i, $\rho(r)$, and $\beta_i(r)$ according eq. 9. This is done numerically, involving three integrations, which are performed with polynomial extrapolations of the integrands up to infinity, s.t. contributions from $\rho(r > r_{max})$ hinders an artificial falloff of $\sigma_{\rm LOS}$. The additional parameter of the slope is calculated from the second half of all bins.

The last step involves comparison of the projected $\nu_i(r)$, $\sigma_i(r)$ and $beta_i(r)$, if available, to the data for the tracer populations to get an error function

$$\chi^2 = \sum_{i=1}^{N} \chi^2_{\nu,i} + \chi^2_{\sigma,i} + \chi^2_{\beta,i} \tag{14}$$

$$\chi^2_{\nu,i} = \sum_{j=1}^{N_{bin}} \left(\frac{\nu_{i,\rm data}(r_j) - \nu_{i,\rm model}(r_j)}{\epsilon_\nu(r_j)} \right)^2 \tag{15}$$

and accordingly for $\chi^2_{\sigma,i}$ and $\chi^2_{\beta,i}$. In absence of a measured $\beta_i(r)$, we set $\chi^2_{\beta,i} = 0$.

The model for iteration $n+1$ is accepted if its close or below the previous iteration,

$$\exp(\chi^2_n - \chi^2_{n+1}) < \varepsilon, \qquad \varepsilon \in [0, 1) \tag{16}$$

for a uniform random ε. Otherwise the model is rejected.

The stepsize can vary for each bin, and is changed during an initialization phase. If the acceptance rate of models lies between 0.24 and 0.26, it is decreased by factors of 1.01, else, it is increased by the same amount. After a burn-in phase of several 100 accepted models with $\chi^2 < \chi^2_{end} = 70$, the stepsize is frozen and the MCMC starts storing the accepted models for further statistical analysis. A default 10^5 models are taken, where nothing else is indicated.

2.1 Binning characteristics

The number of bins for ν, σ, β, ρ are free parameters. They are set to fulfill

$$n_\nu = n_\sigma = n_\beta = n_\rho \leqslant n_{\rm data} \tag{17}$$

with number of datapoints $n_{\rm data}$. This choice simplifies integration greatly, and prevents invention of information on scales smaller than the frequency of datapoints.

(TODO: check that nbin is set s.t.)

$$\chi^2_{red} = \frac{\chi^2}{n_{\rm data} - n_\nu - n_\sigma - n_\beta - n_\rho - 1} \tag{18}$$

is minimized, and still the whole parameter space is tracked.

The whole parameter space for β_i is sampled with $n_\beta = 12$ if $n_{\rm data} = 30$ in the case of 10000 tracers.

The dark matter density is calculated by subtracting the measured baryon density from the dynamical mass density.

2.2 Priors

Following priors are included in the MCMC, and can help to reject unphysical models from the start:

1) cprior: $M(r = 0) = 0$, the central mass is set to 0;
2) bprior: $\rho(r) \geqslant \rho_b(r) - \epsilon_{\rho,b}(r) \forall r \geqslant 0$, ensures that no models with overall densities below the measured baryon density (reduced by the measurement error) are considered any further;
3) lbprior: $M(r > r_{max}) \leqslant M(< r_{max})/3.$, rejects any model which has more than 33% of the overall mass up to the outermost radius in the extrapolated bins;
4) rising ρ prior: $(\rho(r + \Delta r) - \rho(r))/\rho(r) \leqslant 0.5$, prevents ρ rising more than 50% for the next bin. There is no reason for the overall mass density to rise outwards in dynamically old systems. It might be favourable for convergence, though, if a dip in $\rho(r)$ does not lead to immediate rejection of all models with correct $\rho(r + \Delta r)$;
5) $\beta_i(r + \Delta r) - \beta_i(r) < 0.5$: prevent any sudden jumps in β_i;

We show in the appendix what effects the disabling of some of these priors have.

3 TESTS

3.1 Hernquist model

To check the correct function of the integration routine, we used the analytic formulas from Hernquist (1990):

$$M(r) = M\frac{r^2}{(r+a)^2} \quad (19)$$

$$\nu(r) = \frac{M}{2\pi}\frac{a}{r}\frac{1}{(r+a)^3} \quad (20)$$

$$\beta(r) = 0 \quad (21)$$

with mass scale M and length scale a as inputs, and calculated $\sigma_{\rm LOS}(r)$ with our numerical routine, including three integrations. Working with extrapolations to the first bin turns out to give the most stable results, corresponding nicely to the analytic value (Baes & Dejonghe 2002) of

$$\begin{aligned}\sigma_{\rm LOS}(r) &= \frac{1}{I(r)}\frac{1}{24\pi(1-r^2)^3}\times \\ &\quad [3r^2(20-35r^2+28r^4-8r^6)X(r) \\ &\quad +(6-65r^2+68r^4-24r^6)]-\frac{r}{2}, \\ \sigma_r(r) &= r(1+r)^3\ln\left(\frac{1+r}{r}\right) \\ &\quad -\frac{r(25+52r+42r^2+12r^3)}{12(1+r)}, \\ I(r) &= \frac{1}{2\pi}\frac{(2+r^2)X(r)-3}{(1-r^2)^2}, \\ X(r) &= \begin{cases}(1-r^2)^{-1/2}\text{arcsech}\,r, & \text{for } 0\leqslant r\leqslant 1,\\ (r^2-1)^{-1/2}\text{arcsecans}\,r, & \text{for } 1\leqslant r\leqslant\infty\end{cases}.\end{aligned}$$

A single component model is set up according a simple Dehnen split power-law sphere Read et al. (2006),

$$\rho(r) = \frac{M_\infty(3-\gamma)}{4\pi r_S}\left(\frac{r}{r_S}\right)^{-\gamma}\left(1+\frac{r}{r_S}\right)^{4-\gamma}, \quad (22)$$

where $M_\infty = 1$ denotes the total mass, $\gamma = 1$ the logarithmic central asymptotic slope, and $r_S = 1$ the scale length. We use 10^6 sample points, outof which 10^4 are extracted for further analysis.

We then let ν, ρ, β vary. The MCMC correctly recovers the underlying mass distribution.

3.2 Data quality

How many tracer stars are needed to determine the overall density profile reliably? To address this question, we performed three runs with a restricted set of tracer particles. In the first, 10^3 particles were chosen out of the 10^6 simulated particles. With 10^4 particles, the confidence intervals shrink. These 10^4 particles are split then into two populations of each $5\cdot10^3$ particles, with different scalelengths of r_S and $r_S/10$. Most of the second population particles are inside the first two bins, so the overall convergence is not visibly affected above the third bin. However, the models are better constrained around the scalelengths of both tracer populations. This is expected from Walker & Peñarrubia (2011), as any velocity anisotropy sampling yields the same mass constraint there.

4 RESULTS

We apply our method to another set of mock data, the spherical models for the Gaia challenge by Walker and Penarrubia. They consist of dynamical tracer populations with density distribution

$$\nu_*(r) = \nu_0\left(\frac{r}{r_*}\right)^{-\gamma_*}\left[1+\left(\frac{r}{r_*}\right)^{\alpha_*}\right]^{(\gamma_*-\beta_*)/\alpha_*} \quad (23)$$

inside dark matter halos of the form

$$\rho_{\rm DM} = \rho_0\left(\frac{r}{r_{\rm DM}}\right)^{-\gamma_{\rm DM}}\left[1+\left(\frac{r}{r_{\rm DM}}\right)^{\alpha_{\rm DM}}\right]^{(\gamma_{\rm DM}-\beta_{\rm DM})/\alpha_{\rm DM}} \quad (24)$$

with scale radii $r_*, r_{\rm DM}$, inner and outer logarithmic slopes of $\gamma_*, \gamma_{\rm DM}$ and $\beta_*, \beta_{\rm DM}$, with transition parameters $\alpha_*, \alpha_{\rm DM}$.

The anisotropy follows the functional form of **?** and **?**,

$$\beta_{\rm anisotropy}(r) = 1-\frac{\sigma_\theta^2}{\sigma_r^2} = \frac{r^2}{r^2+r_a^2}. \quad (25)$$

with scale radius r_a, turning over from nearly isotropic at $r\to 0$ to radially isotropic at $r_* = r_a$.

Of these distributions, finite samplings are taken and converted to mock observational data including spectral indices, systemic velocities, proper motions, binary motion.

4.1 Cusps and Cores

Applied on a profile with a core in the DM density profile, our method converges fast in the beginning, see fig. 2.

If run for 50000 iterations, the profile in the right plot emerges, with broader errorbars and a slight mismatch above $r_{vir} = 1000$pc.

The model is best constrained around $r = 500$pc, which corresponds to the scale radius of both the stellar tracers.

5 CONCLUSIONS

Conclusions.

6 ACKNOWLEDGEMENTS

JIR would like to acknowledge support from SNF grant PP00P2_128540/1.

REFERENCES

Baes M., Dejonghe H., 2002, A&A, 393, 485
Binney J., Tremaine S., 2008, Galactic Dynamics: Second Edition. Princeton University Press
Breddels M. A., Helmi A., van den Bosch R. C. E., van de Ven G., Battaglia G., 2012, ArXiv e-prints
Cole D. R., Dehnen W., Read J. I., Wilkinson M. I., 2012, MNRAS, 426, 601
de Blok W. J. G., McGaugh S. S., Rubin V. C., 2001, AJ, 122, 2396

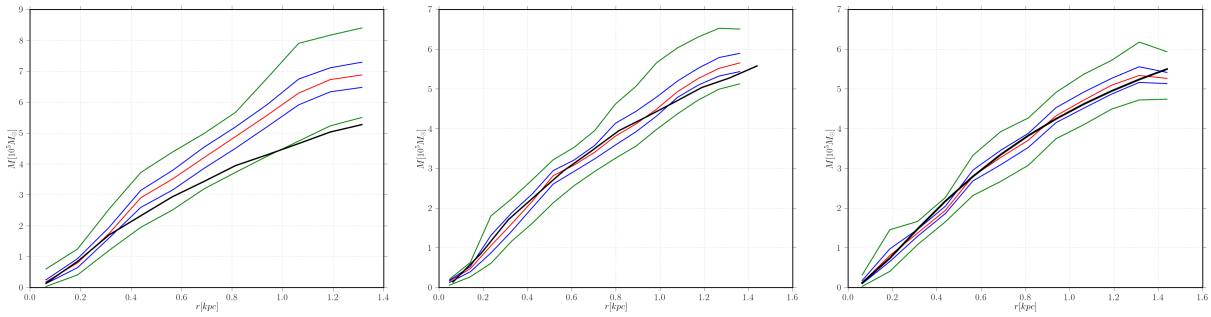

Figure 1. Hernquist profile found by MCMC model (red) for 10^3, 10^4 and 2 times $5 \cdot 10^3$ tracer particles. Black curve shows the enclosed mass derived from model.

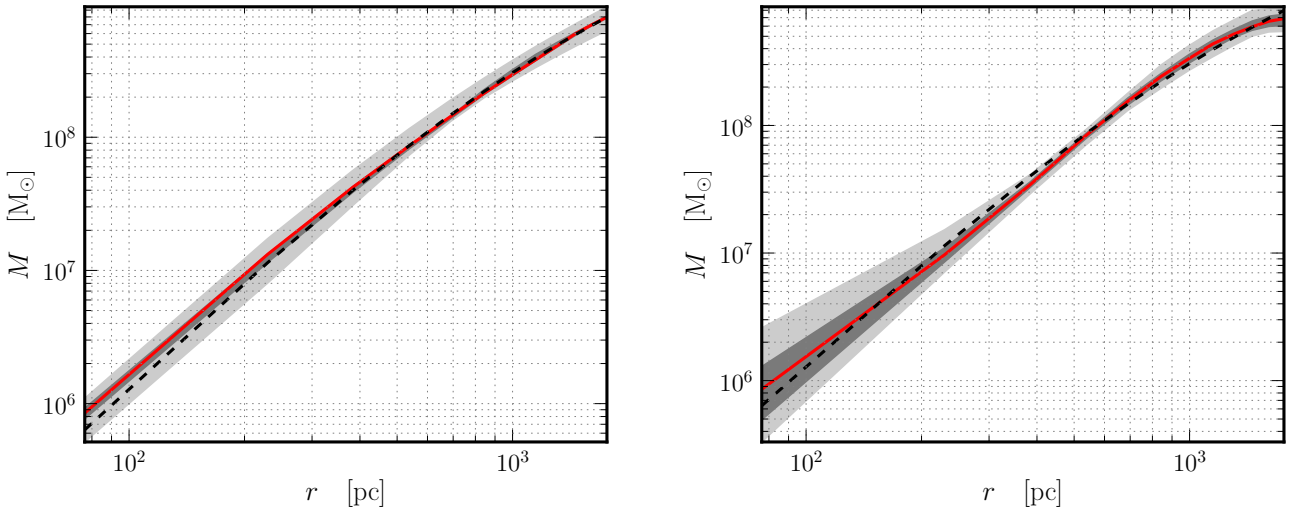

Figure 2. Influence of iteration number: Reconstructed mass of the MCMC model (red shows median, shaded areas are 68 and 90 percentiles) for 10^4 tracer particles, after 1000 iterations (left), and after 50000 (right). The black curve shows the underlying theoretical model.

Goerdt T., Moore B., Read J. I., Stadel J., Zemp M., 2006, MNRAS, 368, 1073
Governato F. et al., 2010, Nature, 463, 203
Hernquist L., 1990, ApJ, 356, 359
Łokas E. L., 2002, MNRAS, 333, 697
Mateo M. L., 1998, ARA&A, 36, 435
McGaugh S. S., Rubin V. C., de Blok W. J. G., 2001, AJ, 122, 2381
Navarro J. F., Frenk C. S., White S. D. M., 1997, ApJ, 490, 493
Oh S.-H., Brook C., Governato F., Brinks E., Mayer L., de Blok W. J. G., Brooks A., Walter F., 2011, AJ, 142, 24
Read J. I., Pontzen A. P., Viel M., 2006, MNRAS, 371, 885
Schwarzschild M., 1979, ApJ, 232, 236
Spergel D. N., Steinhardt P. J., 2000, Physical Review Letters, 84, 3760
Vogelsberger M., Zavala J., Loeb A., 2012, MNRAS, 423, 3740
Walker M. G., Peñarrubia J., 2011, ApJ, 742, 20

7 APPENDIX

7.1 Effects of turning off priors